Measurement Science
and Technology

PAPER • **OPEN ACCESS**

Time-based selection of kaonic atom x-ray events with quasi-hemispherical CZT detectors at the DAΦNE collider

To cite this article: Francesco Artibani *et al* 2026 *Meas. Sci. Technol.* **37** 035108

Measurement Science and Technology

OPEN ACCESS

RECEIVED
8 August 2025

REVISED
22 December 2025

ACCEPTED FOR PUBLICATION
30 December 2025

PUBLISHED
9 January 2026

PAPER

Time-based selection of kaonic atom x-ray events with quasi-hemispherical CZT detectors at the DAΦNE collider

Francesco Artibani[1,2,*], Leonardo Abbene[1,3], Antonino Buttacavoli[1,3], Manuele Bettelli[4], Gaetano Gerardi[3], Fabio Principato[1,3], Andrea Zappettini[4], Massimiliano Bazzi[1], Giacomo Borghi[5,6], Damir Bosnar[1,7], Mario Bragadireanu[8], Marco Carminati[5,6], Alberto Clozza[1], Francesco Clozza[1,10], Raffaele Del Grande[1,11], Luca De Paolis[1], Carlo Fiorini[5,6], Ivica Friscic[7], Carlo Guaraldo[1,†], Mihail Iliescu[1], Masahiko Iwasaki[14], Aleksander Khreptak[1,12,13], Simone Manti[1], Johann Marton[9], Pawel Moskal[12,13], Fabrizio Napolitano[1,15,16], Hiroaki Ohnishi[17], Kristian Piscicchia[1,18], Francesco Sgaramella[1], Michal Silarski[12], Diana Laura Sirghi[1,8,18], Florin Sirghi[1,8], Magdalena Skurzok[1,12,13], Antonio Spallone[1], Kairo Toho[1,17], Lorenzo G Toscano[5,6], Oton Vazquez Doce[1], Johann Zmeskal[9,†], Catalina Curceanu[1] and Alessandro Scordo[1]

[1] Laboratori Nazionali di Frascati, INFN, Via E. Fermi 54, 00044 Frascati, Italy
[2] Dipartimento di Matematica e Fisica, Università di Roma Tre, Via della Vasca Navale 84, 00146 Roma, Italy
[3] Dipartimento di Fisica e Chimica—Emilio Segrè, Università di Palermo, Viale Delle Scienze Edificio 18, 90128 Palermo, Italy
[4] Istituto Materiali per l'Elettronica e il Magnetismo, Consiglio Nazionale delle Ricerche, Parco Area delle Scienze 37/A, 43124 Parma, Italy
[5] Dipartimento di Elettronica, Informazione e Bioingegneria, Politecnico di Milano, Piazza Leonardo da Vinci 32, 20133 Milano, Italy
[6] INFN Sezione di Milano, Via Giovanni Celoria 16, 20133 Milano, Italy
[7] Department of Physics, Faculty of Science, University of Zagreb, Bijenička cesta 32, 10000 Zagreb, Croatia
[8] Horia Hulubei National Institute of Physics and Nuclear Engineering (IFIN-HH), No. 30, Reactorului Street, 077125 Magurele, Ilfov, Romania
[9] Stefan-Meyer-Institut für Subatomare Physik, Dominikanerbastei 16, 1010 Wien, Austria
[10] Dipartimento di Scienze Matematiche Fisiche e Naturali, Università degli Studi di Roma Tor Vergata, Via Cracovia 90, 00133 Roma, Italy
[11] Faculty of Nuclear Sciences and Physical Engineering, Czech Technical University in Prague, Břehová 7, 115 19 Prague, Czech Republic
[12] Faculty of Physics, Astronomy, and Applied Computer Science, Jagiellonian University, Lojasiewicza 11, 30-348 Krakow, Poland
[13] Centre for Theranostics, Jagiellonian University, Kopernika 40, 31-501 Krakow, Poland
[14] RIKEN, 2-1 Hirosawa,Wako, Saitama 351-0198, Japan
[15] Dipartimento di Fisica e Geologia, Università degli studi di Perugia, Via A. Pascoli, 06123 Perugia (PG), Italy
[16] INFN Sezione di Perugia, Via A. Pascoli, 06123 Perugia, Italy
[17] Research Center for Accelerator and Radioisotope Science (RARIS), Tohoku University, 1-2-1 Mikamine, Taihaku-ku, 982-0826 Sendai, Japan
[18] Centro Ricerche Enrico Fermi—Museo Storico della Fisica e Centro Studi e Ricerche 'Enrico Fermi',Via Panisperna 89A, 00184 Roma, Italy
[*] Author to whom any correspondence should be addressed.
[†] Deceased.

E-mail: francesco.artibani@infn.it and francesco.artibani@uniroma3.it

Keywords: timing measurements, CZT detectors, kaonic atoms, x-ray spectroscopy

Abstract

This work presents the results of a time-based event selection for the search of x-ray signals from kaonic atom transitions using a quasi-hemispherical Cadmium–Zinc–Telluride (CZT) detector at the DAΦNE collider. To mitigate the high background level in the measured x-ray spectra, a dedicated event selection strategy was developed, exploiting the precise timing correlation between e^+e^- collisions and detector signals. This approach enabled, for the first time, the observation of two characteristic x-ray transitions from kaonic aluminum atoms with a CZT detector. For the 5–4 transition at 50 keV, 362 ± 41 (stat.) ± 20 (sys.) signal events were observed over 1698 ± 197 (stat.) ± 25 (sys.) background events within $\pm 5\sigma$, with an energy resolution of 9.2% FWHM. For the 4–3 transition at 106 keV, 295 ± 50 (stat.) ± 20 (sys.) signal events were measured over 2939 ± 500 (stat.) ± 16 (sys.) background events, with an energy resolution of 6.6% FWHM. A background suppression of approximately 95% of the triggered data was achieved through this time-based selection. The demonstrated timing capability of the CZT detector proved highly effective

in isolating time-correlated events within an 80 ns window, setting an important benchmark for the application of compound semiconductors in timing-based x-ray spectroscopy. These results highlight the potential of CZT-based detection systems for future precision measurements in high-radiation environments, paving the way for compact, room-temperature x-ray and γ-ray spectrometers in fundamental physics and related fields.

1. Introduction

Nuclear and particle physics experiments require detectors capable of covering a broad energy range while maintaining high energy resolution. Additionally, good timing performance, environmental stability, and resilience to high radiation fluxes over extended periods, especially in collider-based experiments, are essential characteristics for such applications.

In recent years, significant efforts have been devoted to developing compound semiconductors with wide band gaps and high atomic numbers, compared to silicon and germanium detectors, for X and γ-ray detection. One of the main advantages of these materials lies in the possibility of tailoring their physical properties, such as band gap, atomic number, and density, making them highly adaptable to a broad range of applications.

Among compound semiconductors for radiation detection, Cadmium Zinc Telluride (CZT, CdZnTe) has emerged as one of the most promising [1]. This material exhibits high detection efficiency, good energy and time resolutions at room temperature, up to hundreds of keV, making it well suited for experiments in both applied and fundamental research using compact, non-invasive setups [2, 3]. Recent progress in crystal growth, as well as in innovative techniques for electric contacts and data processing [4–7], has made possible to develop new precise systems for x-ray and γ-ray detection using this technology.

The first application of a CZT-based detection system in fundamental particle and nuclear physics was carried out by the SIDDHARTA-2 (Silicon drift detectors for hadronic atom research by timing application) collaboration [8–10] at the DAΦNE collider at Frascati National Laboratories of Istituto Nazionale di Fisica Nucleare (INFN-LNF) by testing, characterizing and using for the first time a CZT-based apparatus to perform intermediate-mass kaonic atoms spectroscopy [11–14].

The experiment exploits the DAΦNE ϕ-factory [15–18] to produce a low-energy charged kaon beam, originating from the decay of the ϕ meson. The kaons are then stopped in a target so that they can bind to a nucleus and form an atomic bound state. The kaonic atom is formed in a highly excited state and undergoes a cascade de-excitation, which is radiative in its final stages. By performing spectroscopic measurements of these transitions, relevant observables can be extracted, crucial for a wide range of topics in fundamental physics, from low-energy strong interaction studies [8, 10, 19–21] and astrophysics [22, 23], to atomic cascade model validations [24, 25] and precision tests of QED [26].

This work represents a significant step forward in demonstrating the feasibility of using this technology under the harsh conditions common in fundamental physics experiments, such as the high radiation flux to which the detectors are exposed and the need to extract signals several orders of magnitude smaller than the background. The deployment of CZT detectors in such settings opens new prospects for compact, room-temperature, and high-resolution detection systems in fundamental physics research.

One of the primary challenges in this application is the suppression of intense background radiation. This elevated background level, typical of collider environments characterized by extremely high event rates, arises from two main sources: beam losses occurring within the accelerator beam pipes (asynchronous background), and radiation directly produced by particle collisions at the interaction point (IP)(synchronous background).

Mitigating the impact of this background requires the development of a detection system capable of discriminating the signal from both synchronous and asynchronous background sources. This necessitates not only dedicated hardware, but also a data selection strategy that fully exploits the timing capabilities of the CZT detectors of the collaboration, allowing for a precise temporal separation between signal and background events. Furthermore, the integration of complementary detection systems operating in coincidence with the CZT modules is essential. These additional systems provide an extra layer of time-based selection, further enhancing the robustness and reliability of the measurement strategy.

In this paper, we present the experimental setup for the CZT-based detectors and the key aspects of the data selection performed on a dataset collected at DAΦNE during the 2024 data-taking campaign. Specifically, the data discussed here were acquired using a single CZT detector between February 28th

and March 20th, 2024, with a total delivered integrated luminosity of 81 pb^{-1}, and a live time of 100%, using an aluminium target.

Section 2 provides an overview of the experimental setup. Section 3 outlines the key steps of the data selection procedure applied to one of the detectors, including relevant findings that confirm the fast timing performance achieved by the CZT detectors. Finally, in section 4, we present a representative energy spectrum from a single run, demonstrating both the effectiveness of the analysis strategy and, for the first time, the observation of kaonic atom transitions with a CZT detector.

2. Experimental setup

2.1. DAΦNE collider

The test measurements were performed at the DAΦNE collider at INFN-LNF. DAΦNE is a unique double-ring electron–positron collider operating at a center-of-mass energy of 1.020 GeV. At this energy, the cross-section for e^+e^- inelastic scattering is dominated by ϕ meson production. The ϕ meson is produced with a slight boost along the axis, directed from the IP inward toward the center of the rings (boost-side), and promptly decays into a pair of back-to-back low-energy charged kaons ($\beta \approx 0.25$), with a branching ratio of 48%. The low-energy negatively charged kaons can thus be easily stopped in a target material, enabling the study of kaonic atoms through the measurement of their cascade transitions. A schematic overview of the main rings of the DAΦNE collider, indicating the SIDDHARTA-2 IP and the location of the CZT detection system used for the measurements described in the following section, is shown in figure 1.

In the DAΦNE collider, the dominant source for the machine-induced experimental background are the effects from intra-bunch electromagnetic interactions producing off-energy particles, which arise when high-density beams are operated at relatively low energies to maximize luminosity (Touschek effect) [28]. A significant fraction of these particles exhibit momentum deviations large enough to prevent them from remaining confined within the nominal beam trajectory. Consequently, they are lost in the focusing magnets before reaching the IP, exiting the beam line, and generating a strong electromagnetic background. The CZT detection system is located near the focusing magnets in front of the IP, and in this region, the background is particularly intense, posing a major challenge for precision measurements and requiring an accurate analysis for background reduction.

2.2. The CZT detection system

The SIDDHARTA-2 experiment was installed at the only active IP of the DAΦNE collider, highlighted in figure 1. The main experimental setup employed Silicon drift detectors (SDDs) [29–31] to study kaonic atom transitions from light-mass, cryogenic targets, with x-ray energies ranging from a few keV up to several tens of keV. A detailed description of the setup can be found in [32].

The primary SIDDHARTA-2 apparatus was arranged above and below the IP, featuring a sophisticated system composed of multiple detectors. Due to the limited space available only in the plane of the collider's beam pipe, a compact detection system was required to extend the measurements to kaonic atom transitions of intermediate-mass elements, which emit x-rays in the energy range from tens to hundreds of keV. For this purpose, CZT-based detectors were employed to test and demonstrate the effectiveness of the new technology in this field and to complement the SDD measurements.

During the data-taking campaign, the CZT detectors were placed in the boost side of DAΦNE's IP, on the plane of the collider rings. Moving outward from the IP, the boost-side luminometer (LUMI) was positioned first. This module consists of an 80 mm × 40 mm × 2 mm Scionix BC-408 organic scintillator coupled to two PMTs [33] through plastic lightguides. Used in combination with an identical module on the antiboost side, the LUMI served both for luminosity measurements and for charged kaon selection via time-of-flight (see section 3), and was located 10.2 cm from the IP. Immediately after the LUMI, a solid target was placed, in which the kaons stopped and formed atomic states with the nuclei of the target material. In the run presented in this work, an aluminum target was used. Finally, the x-rays emitted by the kaonic atoms were detected by the CZT system, composed of eight 13 mm × 15 mm × 5 mm quasi-hemispherical CZT detectors grown using traveling heater method by REDLEN Technology (Canada), enclosed in a thin aluminum box with a 0.27 μm thick aluminum window, housing both the active detector material and the front-end electronics. Each detector is characterized by a rectangular electrode (3.8 × 1.8 mm^2) on the anode side, while the cathode electrode covers the full crystal area (13 × 15 mm^2). Gold electroless contacts were realized for both the cathode and the anode electrodes. The detectors were positioned 17 cm from the target. A schematic view of the setup is shown in figure 2.

Each CZT detector in the system was connected to a custom front-end electronic chain based on analog charge-sensitive preamplifiers (CSPs) [11, 34]. The CSPs are characterized by an equivalent noise

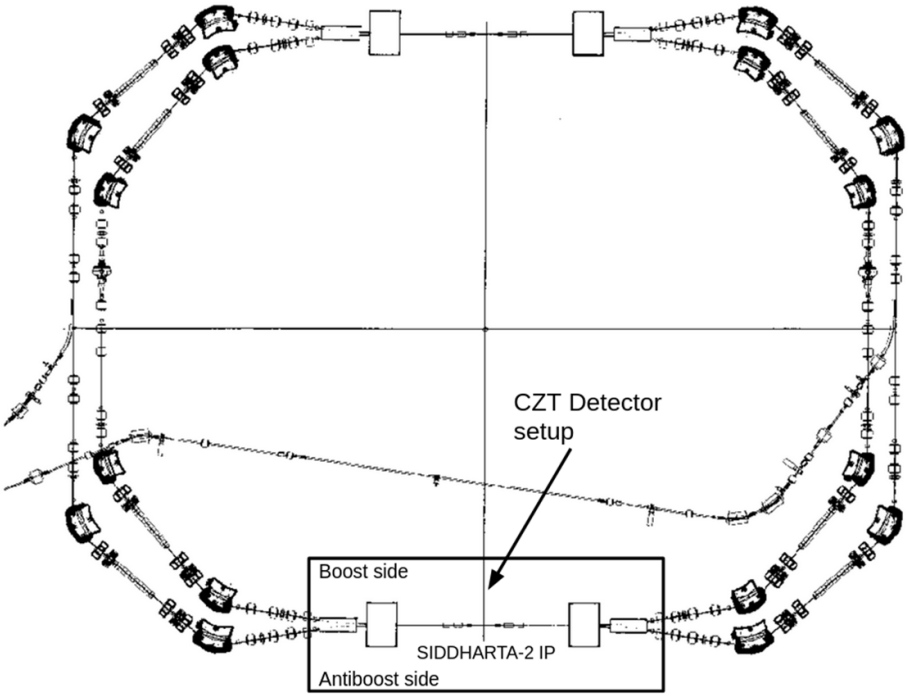

Figure 1. Schematic areal view of the main rings of DAΦNE collider. The SIDDHARTA-2 interaction point, together with the CZT detection system setup, is highlighted. Reproduced from [27] CC BY 3.0.

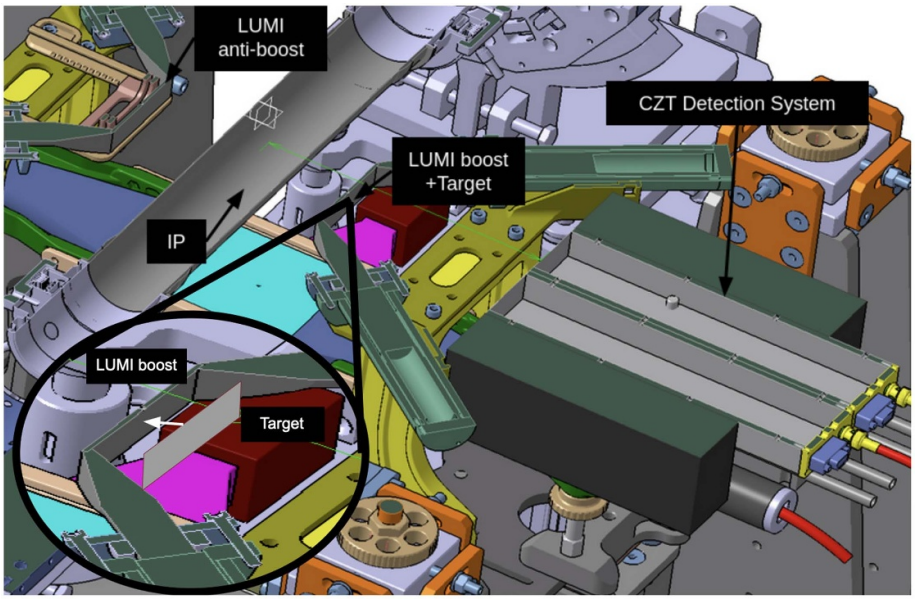

Figure 2. Schematic view of the experimental setup of the CZT detection system in DAΦNE. A description of the materials follows: The DAΦNE beam pipe (around the IP in the figure, displayed in grey) is made by a mixture of aluminum and carbon fiber; the LUMI detectors (housing and lightguides shown wrapped in aluminized mylar, coloured in silver); the Target (shown in light gray) is an aluminum plate; the CZT detection system's box (displayed in light grey) is made of aluminum; mechanical supports and mounting structures (brackets yellow, kinematic mounts orange) are made of aluminum alloy. Additional small components visible: an electronics/power module (magenta) and support plates (cyan/turquoise).

charge of about 100 electrons (equivalent to about 1 keV FWHM for CZT detectors) and equipped with a resistive-feedback circuit with exponential decay and time constant of 100 μs. A dedicated digital acquisition system recorded, in real time, the output waveforms from all eight detectors. The acquired data consisted of sets of snapshot waveforms (SWs) per detector channel, where each pulse was time-stamped using the single delay line shaping technique.

The SWs were later analyzed offline within a dedicated LabView-based framework, developed to extract pulse characteristics and generate energy spectra. Each snapshot covered a time window of 10 μs,

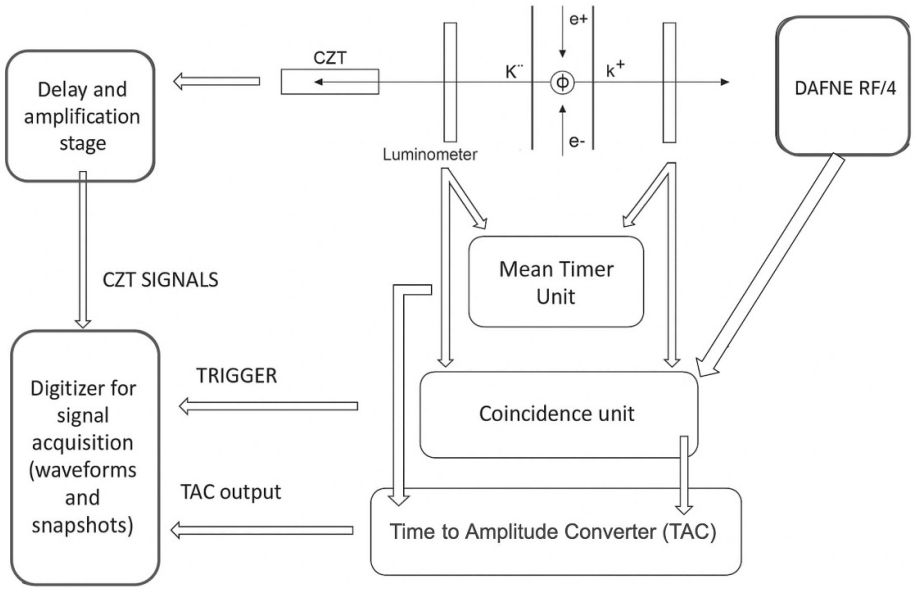

Figure 3. Schematic view of the DAQ system of the experiment. Reprinted from [12], Copyright (2023), with permission from Elsevier.

which can be considered the actual dead time of the process. This configuration ensures a high throughput, defined as the ratio of output to input counting rate, reaching 99% up to an ICR of 1500 cps, which is the highest rate measured during beam-on conditions. A detailed description of the data acquisition and processing is reported in previous works [11, 34].

2.3. The DAQ logic

The DAQ logic was based on a setup already employed and described in a previous study [12]. The signals from the two LUMI scintillators were processed by an ORTEC 935 constant fraction discriminator and then sent to a CAEN N93B mean timer unit. The output of the Mean Timer was used as the stop signal for an ORTEC 566 Time-to-amplitude converter (TAC), while the start signal was provided by a triple coincidence between the DAΦNE radiofrequency (RF)/4 clock and the LUMI signals, generated using a CAEN N455 coincidence unit. The data in this run were acquired in trigger mode, meaning that the signals on the detectors were recorded each time there was a coincidence between the two TAC and the DAΦNE collider RF signal.

The TAC output was a signal with an amplitude proportional to the time difference between start and stop, and it was sent to the same digitizer that recorded the CZT signals. Both the TAC and CZT outputs were acquired by a digitizer controlled by a custom firmware developed at the University of Palermo. In addition to waveform acquisition, the digitizer also provided the time of arrival of each signal relative to the TAC output.

A scheme of the DAQ system can be found in figure 3.

3. Data selection

This work introduces a data selection strategy that exploits the timing capabilities of CZT-based detectors. Combined with the two LUMI for time-of-flight selection, these detectors proved to be well suited for kaonic atom spectroscopy and, more broadly, for accelerator-based fundamental physics research where background reduction is essential. To this goal, we describe the optimization of data selection performed on the dataset acquired with one of the eight quasi-hemispherical CZT detectors employed in the experiment.

After summarizing the CZT energy calibration method, we present the approach used to maximize the signal significance (Z) and how it is applied to the selection of kaon-related signals on one of the detectors. This selection is enabled by the LUMI system, as already explored in previous works [11, 12], and is also used to study and exploit the distribution of the time difference between the detector signal and the trigger (Δt). Finally, we present the resulting spectrum obtained with the optimized cut and evaluate the background rejection factor achieved through this methodology. A schematic flowchart of the data selection process can be found in figure 4 .

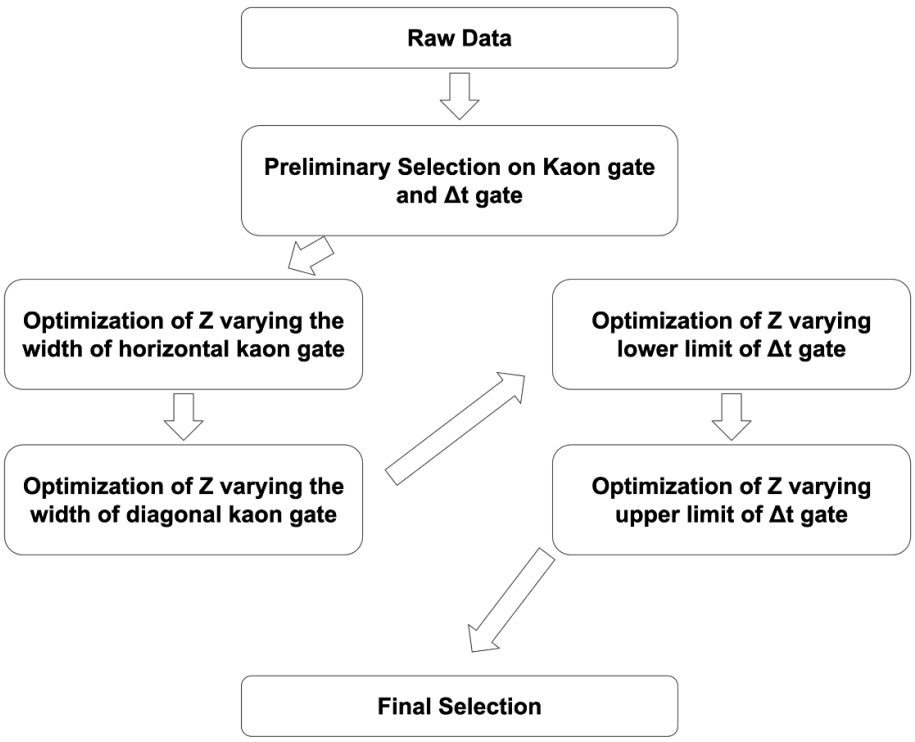

Figure 4. Scheme of the data selection optimization process described in the section.

3.1. Energy calibration method

The calibration used for the dataset analyzed in this work was performed on March 5th, 2024, in the middle of the data-taking run. The calibration procedure for the CZT detector has been thoroughly described in a previous work [34].

The detector calibrated with this method demonstrated good energy stability across the entire data-taking period, confirming the reliability of the system and its resistance to potential issues arising from electronics or environmental conditions.

For a more detailed discussion of the calibration method, the *a priori* estimation of systematic errors, and the results on the system's energy stability, we refer the reader to our previous work [34].

3.2. Kaon-minimum ionizing particles(MIPs) discrimination

The signals from the two LUMI scintillators, combined with the DAΦNE collider RF signal, can be used to discriminate charged kaon pairs originating from the IP [11, 12]. The narrow momentum spread and low β of the kaons from ϕ meson decays allow for the selection of kaon-related signals through time-of-flight measurements. The TAC-processed LUMI used in the experiment was shown to effectively distinguish between kaons and MIPs [11, 12]. For the 2024 run, the combined signal from both the boost side and antiboost side LUMIs was employed, representing a significant improvement in kaon pair discrimination capability.

Figure 5 shows the spectrum of the two LUMI signals after TAC processing and their combined 2D histograms. The narrower peaks correspond to the kaon windows, due to the smaller momentum spread compared to MIPs. Four similar patterns, corresponding to kaon and MIP arrivals, appear because the TAC operates at a frequency of 1/4 of the DAΦNE RF, which is 3.7 MHz [15–18].

In this work, the two time windows for kaon selection were optimized to maximize the signal significance (Z), defined as:

$$Z = \frac{A_S}{\sqrt{A_B}}, \tag{1}$$

where A_S is the number of events in the Gaussian peak representing the signal, and A_B is the number of background events in the same energy region.

After a Δt cut (see next section), to select only the events on the detector correlated in time with the collisions and remove the asynchronous background, the time-of-flight selection was optimized by calculating the signal significance for different time windows. This yielded a distribution of Z as a function of

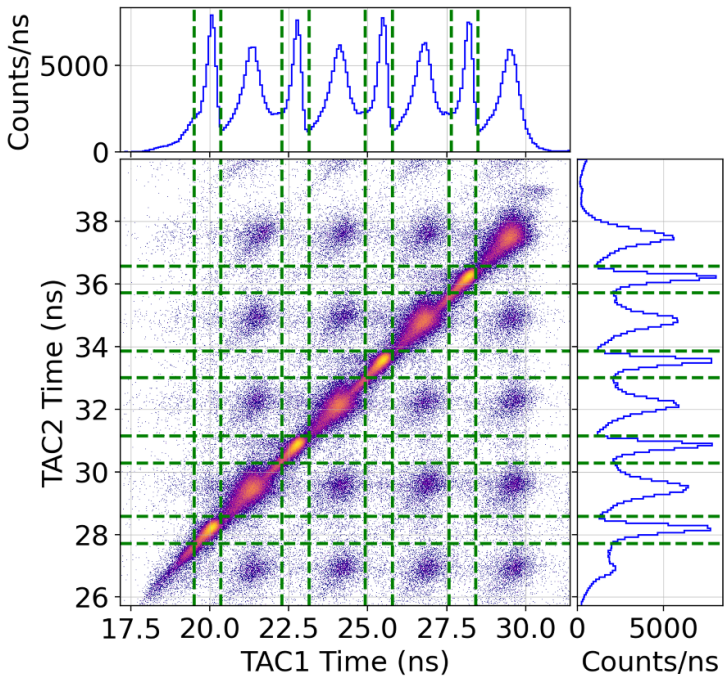

Figure 5. 2D histogram of TAC1 vs TAC2. Kaon-related coincidences appear as narrow peaks within the green guidelines.

the selected kaon region, from which the optimal window, corresponding to the maximum Z, was identified. The optimization was performed by fixing the right-hand boundaries of the two TACs (where the signal starts to rise, as shown in figure 5), while progressively extending the other boundaries to enlarge the kaon window. For each configuration, an energy spectrum was extracted and fitted to evaluate the visible signal, and Z was computed following equation (1).

A similar approach was applied using a linear window in the TAC1 vs TAC2 plane, in which the window width was varied while its center remained fixed. This method allowed the identification of the time-of-flight selection region that maximizes signal significance while effectively suppressing background.

The fitting procedure and details of the signal significance calculation are described below. The number of signal events was determined by fitting the visible kaonic atom transitions in the energy spectrum—specifically the K-Al 5→4 (50 keV) and 4→3 (106 keV) transitions—with Gaussian functions. The means were fixed to values calculated using the MCDFGME code [35], and the standard deviations were modeled as a function of energy:

$$\sigma(E) = \sqrt{a + bE} \tag{2}$$

following [36], with the parameters a and b fixed to values determined from detector calibration. The areas of the peaks were left as the only free parameters.

The background was modeled using a combination of an exponential term, a complementary error function, and a linear term, following the approach in [34]:

$$f_{\text{bkg}}(x) = a + b \cdot x + c \cdot \exp(d \cdot x) + \operatorname{erfc}\left(\frac{e - x}{f}\right). \tag{3}$$

where a and b are the parameters of the linear function describing the electronic baseline; c and d are the parameters of the exponential component accounting for the background generated by photons and electrons undergoing Compton scattering; e and f are the two parameters of the complementary error function, which accounts for the low-energy cutoff resulting from the presence of shielding and electronic components. The exponential term for Compton scattering arises from the fact that the particles from the IP interact with the air and the materials between the beam pipe and the detector, producing a considerable number of secondary particles at lower energies.

Two additional background peaks originating from lead fluorescence were included. In particular, the lead Kα transition required an extra component to account for incomplete charge collection. This was

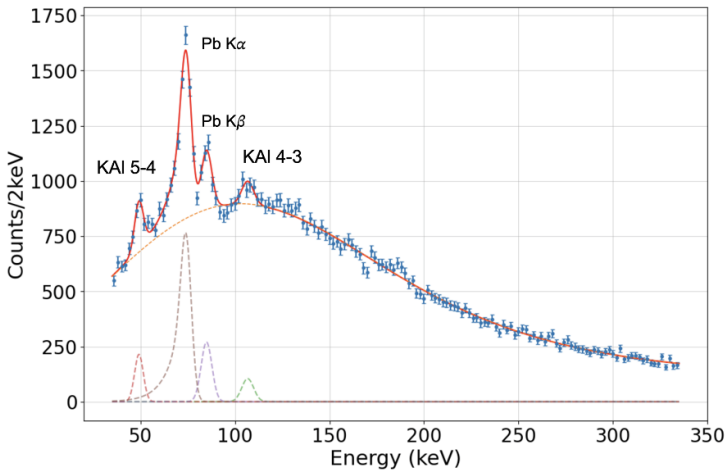

Figure 6. One of the fits to the distribution of events per energy in one CZT detector, used to quantify the signal significance of the kaonic aluminum peaks with the different cuts. The K-Al transitions, the background in equation (3), and the two background peaks due to lead fluorescence are shown together with the total fit. The errorbars represent the statistical errors on the number of counts N ($1/\sqrt{N}$).

modelled using an exponential function multiplied by a complementary error function:

$$T(x) = \epsilon \times N \times \exp\left(\frac{x-\mu}{\beta\sigma}\right) \times \mathrm{erfc}\left(\frac{x-\mu}{\sqrt{2}\sigma} + \frac{1}{\sqrt{2}\beta}\right), \tag{4}$$

where μ and σ are the mean and standard deviation of the corresponding Gaussian, ϵ controls the tail amplitude, and β defines its width. This model was introduced and validated in [34]. Tail parameters were fixed to calibration values, and the incomplete charge collection effect was negligible in all other peaks.

The full background model, including tail components, was also validated during a dedicated run with the DAΦNE collider operating, as reported in [34].

In figure 6, a plot showing one of the fits done for optimizing the kaon time-of-flight window is reported, with the KAl and lead transition labeled.

The Zs for the two K-Al peaks in each time window were then obtained by extracting from the fit the area of the Gaussians representing the signal and the corresponding background area in the region between $\mu - 5\sigma$ and $\mu + 5\sigma$ underneath them—with μ representing the mean of the Gaussian, and σ the standard deviation—and finally applying equation (1).

After obtaining the Z distributions as a function of the varied boundary values (as shown in figure 7), an arbitrary maximum Z value within the region of highest values was selected to define the final limit used for the cut. The reported errors correspond to the statistical uncertainties on the signal amplitude, which represent the dominant contribution.

The final selection applied to TAC1 and TAC2 for one of the four patterns (see the 2D histogram in figure 5) is shown in figure 8. The green box indicates the optimized region corresponding to the maximum achievable Z, as determined by the procedure described above.

3.3. Timing analysis

In kaonic atom spectroscopy at DAΦNE, as demonstrated by the SIDDHARTA and SIDDHARTA-2 experiments [8, 9, 37], the time distribution of detector signals plays a crucial role in applying time-based cuts. In particular, a clear time correlation exists between the signals originating from kaon production and the collisions, which manifests as a peak in the distribution of the time difference between the trigger and a detector signal (Δt). By selecting events within this peak region, it is possible to significantly reduce the background from uncorrelated processes, thereby enhancing the signal quality.

In previous works, CZT detectors demonstrated ideal timing capabilities for kaonic atom measurements. In particular, the characteristic peak in the distribution of the difference between the CZT signal time and the trigger time (Δt), corresponding to the beam-related events, was observed [12]. In the run analyzed in this work, the timing distribution proved again to be promising, showing the expected excess in the Δt spectrum.

The final Δt window was chosen after applying the same method used for the time-of-flight selection, choosing the time window in which the signal significance is higher. At first, the upper limit was

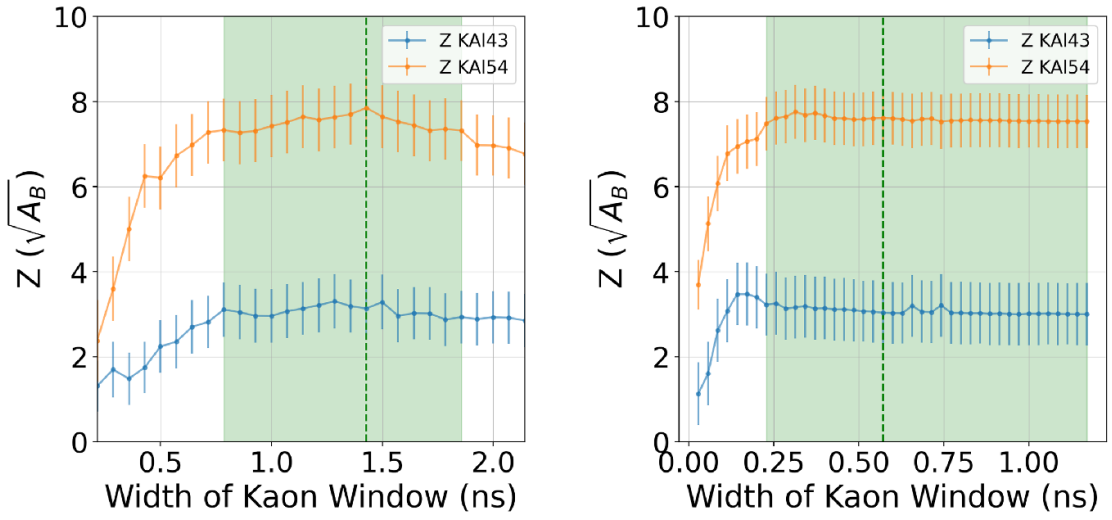

Figure 7. Left: Z distribution as a function of the TAC kaon selection width, with the selected maximum value (100 ADC TAC) marked by the green line and the maximum region highlighted in green. Right: Z distribution as a function of the selection width in the TAC1 vs TAC2 space, with the selected maximum value (40) marked by the green line and the maximum region highlighted in green. The reported errors correspond to the statistical uncertainties on the signal amplitude.

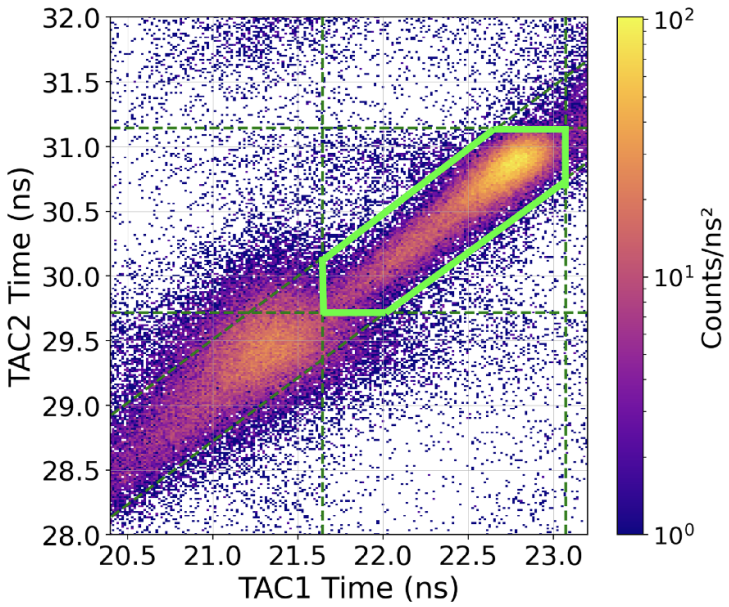

Figure 8. 2D histogram of the two TAC signals from the LUMI scintillators for one kaon-MIP couple, with the optimized selection guidelines shown as dotted green lines. The selected kaon windows correspond to the hexagonal areas formed by the broader rectangles along the diagonal, combined with the region inside the diagonal cuts. These selected area is highlighted in light green in the figure.

fixed to a high value of 300 ns, and the lower limit was varied to obtain the Z distribution. Subsequently, the lower limit was fixed to the optimal value, and the upper limit was varied to obtain the distribution of the Z. The two distributions are reported in figures 9(a) and (b) respectively.

In the first distribution, the maximum value is reached around ≈ -10 ns, which corresponds to the chosen lower limit of the window. In the second one, the maximum is found around 70 ns, after which a plateau is observed for the 5–4 transition, less affected by background. This value corresponds to the chosen upper limit of the window. This study confirms that the evident peak around -10 ns is due to the synchronous background, while the signal related to kaonic atoms spans the wider time window. The optimized kaon window limits, highlighted in green, are reported in figure 10. The dominant contribution to the observed width of the Δt distribution arises from the charge drift time within the CZT detector: a kaon with $\beta \approx 0.25$ covers the 10.2 cm between the IP and the target in about 2 ns, while the timescales for kaon capture, atomic cascade, and x-ray emission range from 10^{-12} s to 10^{-9} s. Likewise,

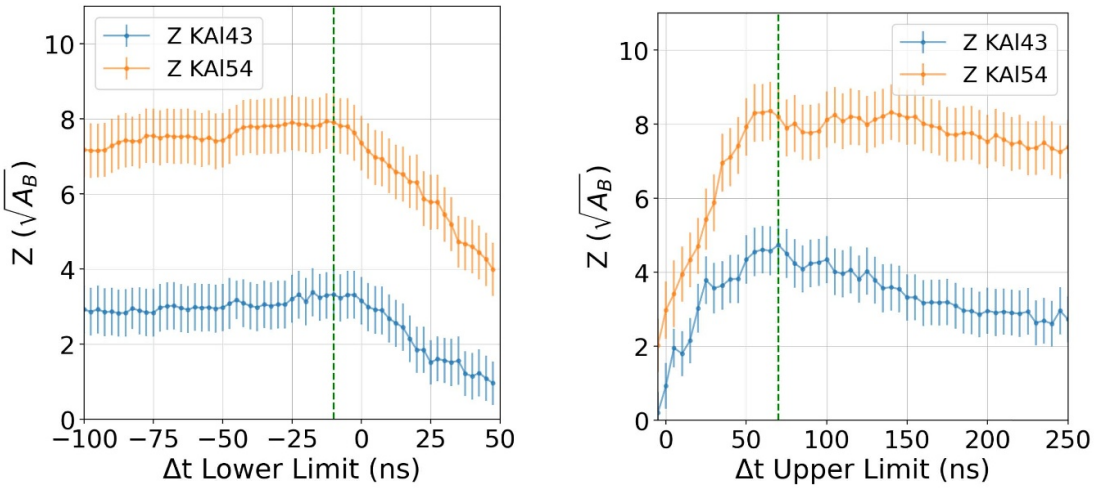

(a) Z vs lower limit of Δt (upper limit fixed at -10 ns).

(b) Z vs upper limit of Δt (lower limit fixed at 70 ns).

Figure 9. Left: Z distribution in function of lower limit of Δt with upper limit fixed at 300 ns. The maximum is highlighted in green (-10 ns). Right: Z distribution in function of upper limit of Δt with lower limit fixed at 10 ns. The maximum is highlighted in green (70 ns). The reported errors correspond to the statistical uncertainties on the signal amplitude.

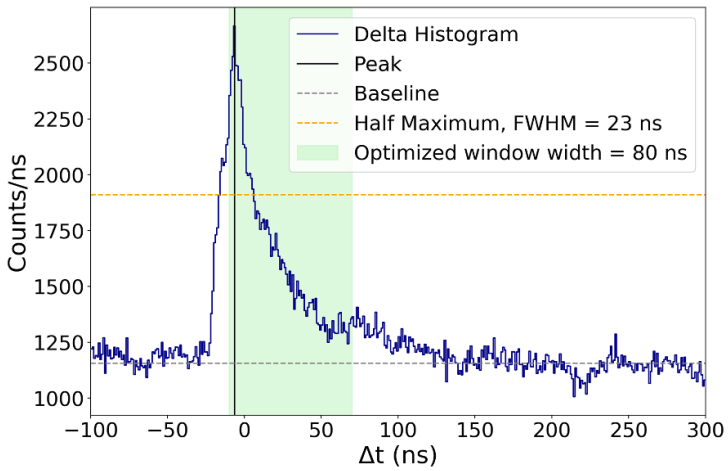

Figure 10. Measured cumulative spectrum of the drift time with the optimized limits of the signal region reported in green. In the legend the FWHM of the peak and the width of the selected window are reported.

the photon flight time over the 9 cm from the target to the detector is less than 1 ns. The contribution of these processes to the overall Δt width is therefore well below the nanosecond level and can be considered negligible. Consequently, the measured FWHM can be regarded as a direct measurement of the detector's intrinsic time resolution, obtained using x-rays and particles spanning a wide range of energies. Overall, a dedicated study performed in a low-background environment with a monochromatic photon source would provide a more precise characterization.

A $\approx$ 100 ns Δt window gives a very good result, compared to that achieved with the SDDs used in the experiment [(507.60 $\pm$ 0.47) ns at FWHM] [38]. This finding demonstrates the remarkable potential of CZT detector timing for background reduction in high-radiation environments.

4. Final selected spectrum

The spectrum with kaon and Δt selections, acquired by the CZT detection system, compared with the raw spectrum, is reported in figure 11.

After the two selection steps, approximately 95% of the triggered events are discarded. In a previous study [39], the overall rejection factor for total events was evaluated using the coincidence of a kaon signal on a single LUMI scintillator and a variable Δt window. That work showed that, within a 100 ns Δt

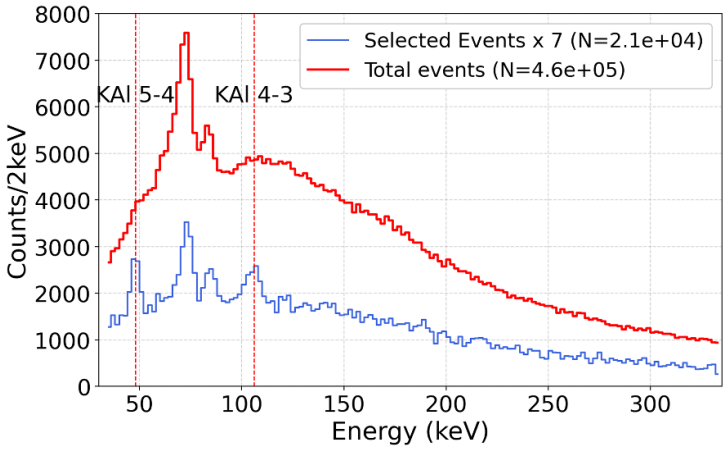

Figure 11. Histogram of the raw spectrum (red), compared to the one after the optimized selections with counts multiplied by a factor 7 (blue), with the kaonic aluminum transitions highlighted in red.

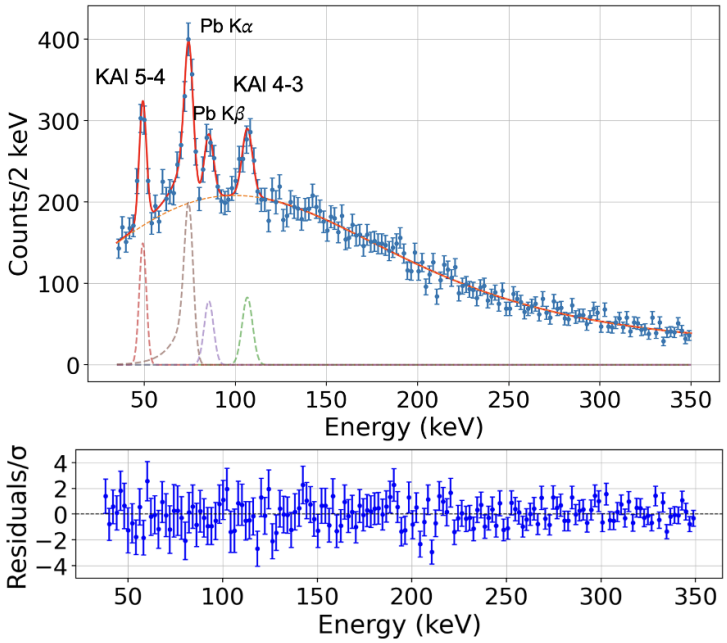

Figure 12. Fit to the data after the optimized selection (up). The errors of the number of counts reported are the statistical errors ($1/\sqrt{\text{counts}}$). The plot of residuals for each bin normalized at their standard deviation (σ) is also reported (down).

window, the rejection factor relative to the total number of triggered and untriggered events was on the order of 10^6, a comparable rejection efficiency is expected when considering the total number of events on the detector. These findings further confirm the method's strong background suppression capability, highlighting its potential for future precision measurements in high-radiation environments.

In the spectrum, two kaonic aluminum transitions, KAl 5–4 (50 keV), and KAl 4–3 (106 keV), are visible, confirming the robustness of both the analysis and the detection system.

To confirm the successful observation of the two transitions, a final fit was performed on the dataset. The fitting procedure was the same as described in section 3. In this final fit, the two parameters describing the detector's energy resolution and the two parameters modeling the incomplete charge collection for the Pb Kα transition were left free, in order to avoid bias and to determine the final resolution after the cuts. The resulting fit, together with the residuals, is reported in figure 12.

The measured resolutions at 50 keV and 106 keV are respectively (FWHM/nominal value) 9.2 % 50 keV and 6.3% at 106 keV, compatible with the ones reported in previous works [12, 34].The resulting peaks and background area with the corresponding Z value are reported in table 1.

Table 1. Table reporting the number of signal events, background events and Z value obtained from the final fit fo the two transitions.

ine Transition	Signal events	Background events ($\pm 5\sigma$)	Significance (Z)
ine KAl 5–4	362 ± 41 (stat.) ± 20 (sys.)	1698 ± 197 (stat.) ± 25 (sys.)	8.78 ± 1.13 (stat.) ± 0.49 (sys.)
KAl 4–3 ine	295 ± 50 (stat.) ± 20 (sys.)	2939 ± 500 (stat.) ± 16 (sys.)	5.44 ± 1.03 (stat.) ± 0.41 (sys.)

The systematic uncertainties were evaluated as follows:

1. Four additional fits were performed by shifting the calibration gain and offset by 0.0015 and 0.075, respectively. According to calibration studies reported in [34] , these values correspond to the expected variations over several tens of days. The systematic uncertainty from this effect was estimated by taking the quadratic sum of the deviations from the nominal values after applying the gain and offset shifts.
2. Two additional fits were carried out by varying the energy window limits by ± 5 keV (upper limit) and ± 1 keV (lower limit), and the resulting differences were used to estimate the related systematic contribution.
3. One additional fit was performed modifying the background model by removing the linear term (parameter b in equation (3)).
4. The binning was varied by ± 5 channels, and the corresponding variation in the fitted results was recorded.
5. Finally, the total systematic uncertainty was obtained by adding in quadrature the contributions from all the sources listed above.

The most relevant systematic contributions to the number of events arise from the gain variation (point 1) and the choice of binning (point 4).

The observed Z and energy resolution are sufficient to resolve the individual lines, demonstrating the good timing and spectral performance of the CZT detectors, even within the challenging conditions of an accelerator-based experiment.

This method will be applied to the analysis of the full kaonic aluminum dataset, as well as to the measurements acquired with different targets during the 2024 data-taking campaign, which are expected to provide new results in intermediate-mass kaonic atom spectroscopy.

5. Conclusions

In this paper, we presented the data selection procedure and the first x-ray spectrum acquired by a single CZT detector (out of an array of eight) tested by the SIDDHARTA-2 collaboration during a 20 d run with an aluminum target.

After briefly describing the experimental setup and calibration methods, we discussed the optimization of the kaon selection window and the time difference window between the trigger and the detector signal, aimed at maximizing the signal significance Z.

We demonstrated that most of the kaonic-aluminum signal is concentrated within a time window of 80 ns from the trigger, confirming the excellent timing performance of CZT detectors for background suppression.

The resulting energy spectrum, after applying all selection criteria, clearly shows the first observed kaonic-aluminum transition peaks using a room-temperature detector. The significance values calculated using equation (1) were 5.45 ± 1.03 (stat.) ± 0.41 (sys.) for the 4–3 transition at 106 keV, and 8.79 ± 1.13 (stat.) ± 0.49 (sys.) for the 5–4 transition at 50 keV, with corresponding energy resolutions (FWHM/nominal energy) of 9.2% and 6.3%, respectively. These results demonstrate both the effectiveness of the CZT-based detection system developed by the SIDDHARTA-2 collaboration and the feasibility of precision kaonic atom spectroscopy with CZT detectors.

This work establishes a validated data selection strategy for CZT detectors and represents a proof of concept for future measurements of intermediate-mass kaonic atoms using CZT-based systems. The present analysis was performed on the data acquired by a single detector in a short test run, while the same methodology will be applied to the full dataset collected at DAΦNE during the 2024 campaign. Finally, this study paves the way for new applications of CZT detectors in kaonic-atom spectroscopy, both at DAΦNE and at J-PARC, demonstrating their strong potential for precision measurements in challenging experimental environments.

Data availability statement

All data that support the findings of this study are included within the article (and any supplementary files).

Acknowledgments

We thank H Schneider, L Stohwasser, and D Pristauz-Telsnigg from Stefan Meyer-Institut for their fundamental contribution in designing and building the SIDDHARTA-2 setup. We thank as well the INFN, INFN-LNF and the DAΦNE staff in particular to Dr Catia Milardi for the excellent working conditions and permanent support. Catalina Curceanu acknowledge University of Adelaide, where part of this work was done (under the George Southgate fellowship, 2024).

Funding

Part of this work was supported by the Austrian Science Fund (FWF): [P24756-N20 and P33037-N]; the Croatian Science Foundation under the project HRZZ-IP-2022-10-3878; the EU STRONG-2020 project (Grant Agreement No. 824093); the EU Horizon 2020 project under the MSCA (Grant Agreement 754 496); the Japan Society for the Promotion of Science JSPS KAKENHI Grant No. JP18H05402; the SciMat and qLife Priority Research Areas budget under the program Excellence Initiative—Research University at the Jagiellonian University, and the Polish National Agency for Academic Exchange (Grant No. PPN/BIT/2021/1/00037); the EU Horizon 2020 research and innovation programme under project OPSVIO (Grant Agreement No. 101038099). This work was also supported by the Italian Ministry for University and Research (MUR), under PRIN 2022 PNRR project CUP: B53D23024100001.

Author contributions

Francesco Artibani 0009-0000-8905-3165
Data curation (equal), Formal analysis (equal), Software (equal), Writing – original draft (equal)

Leonardo Abbene
Data curation (equal), Resources (equal), Software (equal), Writing – review & editing (equal)

Antonino Buttacavoli
Data curation (equal), Resources (equal), Software (equal), Writing – review & editing (equal)

Manuele Bettelli
Resources (equal), Writing – review & editing (equal)

Gaetano Gerardi
Software (equal), Writing – review & editing (equal)

Fabio Principato 0000-0003-2787-0877
Resources (equal), Software (equal), Writing – review & editing (equal)

Andrea Zappettini 0000-0002-6916-2716
Resources (equal), Writing – review & editing (equal)

Massimiliano Bazzi
Writing – review & editing (equal)

Giacomo Borghi
Writing – review & editing (equal)

Damir Bosnar 0000-0003-4784-393X
Writing – review & editing (equal)

Mario Bragadireanu
Writing – review & editing (equal)

Marco Carminati
Writing – review & editing (equal)

Alberto Clozza
Writing – review & editing (equal)

Francesco Clozza 0009-0002-3298-0624
Writing – review & editing (equal)

Luca De Paolis
Writing – review & editing (equal)

Carlo Fiorini
Writing – review & editing (equal)

Ivica Friscic 0000-0002-4743-0572
Writing – review & editing (equal)

Carlo Guaraldo
Conceptualization (equal)

Mihail Iliescu
Writing – review & editing (equal)

Masahiko Iwasaki
Writing – review & editing (equal)

Aleksander Khreptak 0000-0002-9482-9770
Writing – review & editing (equal)

Simone Manti
Writing – review & editing (equal)

Johann Marton
Writing – review & editing (equal)

Pawel Moskal 0000-0002-4229-3548
Writing – review & editing (equal)

Fabrizio Napolitano 0000-0002-8686-5923
Writing – review & editing (equal)

Hiroaki Ohnishi
Writing – review & editing (equal)

Kristian Piscicchia
Writing – review & editing (equal)

Francesco Sgaramella 0000-0002-0011-8864
Writing – review & editing (equal)

Michal Silarski
Writing – review & editing (equal)

Diana Laura Sirghi
Writing – review & editing (equal)

Florin Sirghi
Writing – review & editing (equal)

Magdalena Skurzok
Writing – review & editing (equal)

Antonio Spallone
Writing – review & editing (equal)

Kairo Toho
Writing – review & editing (equal)

Lorenzo G Toscano
Writing – review & editing (equal)

Oton Vazquez Doce
Writing – review & editing (equal)

Johann Zmeskal
Resources (equal)

Catalina Curceanu
Resources (equal), Supervision (equal), Validation (equal), Writing – review & editing (equal)

Alessandro Scordo 0000-0002-7703-7050
Conceptualization (equal), Data curation (equal), Methodology (equal), Resources (equal), Software (equal), Supervision (equal), Writing – review & editing (equal)

References

[1] Sordo S D, Abbene L, Caroli E, Mancini A M, Zappettini A and Ubertini P 2009 Progress in the development of CdTe and CdZnTe semiconductor radiation detectors for astrophysical and medical applications *Sensors* **9** 3491–526
[2] Iniewski K 2014 CZT detector technology for medical imaging *J. Instrum.* **9** C11001
[3] Tang J, Kislat F and Krawczynski H 2021 Cadmium zinc telluride detectors for a next-generation hard x-ray telescope *Astropart. Phys.* **128** 102563
[4] Abbene L, Gerardi G, Raso G, Basile S, Brai M and Principato F 2013 Energy resolution and throughput of a new real time digital pulse processing system for x-ray and gamma ray semiconductor detectors *J. Instrum.* **8** 07019
[5] Abbene L, Gerardi G, Raso G, Principato F, Zambelli N, Benassi G, Bettelli M and Zappettini A 2017 Development of new CdZnTe detectors for room-temperature high-flux radiation measurements *J. Synchrotron. Rad.* **24** 429–38
[6] Abbene L *et al* 2020 Room-temperature x-ray response of cadmium-zinc-telluride pixel detectors grown by the vertical bridgman technique *J. Synchrotron Rad.* **27** 319–28
[7] Vicini V, Zanettini S, Amade N S, Grill R, Zambelli N, Calestani D, Zappettini A, Abbene L and Bettelli M 2023 Optimization of quasi-hemispherical cdznte detectors by means of first principles simulation *Sci. Rep.* **13** 3212
[8] Curceanu C *et al* 2019 The modern era of light kaonic atom experiments *Rev. Mod. Phys.* **91** 025006
[9] Artibani F *et al* 2024 The odyssey of kaonic atoms studies at the DAΦNE collider: from dear to SIDDHARTA-2 *Acta Phys. Polon. B* **55** 5–A2
[10] Curceanu C *et al* 2023 Kaonic atoms at the DAΦNE collider: a strangeness adventure *Frontiers Phys.* **11** 1240250
[11] Abbene L *et al* 2023 Potentialities of CdZnTe quasi-hemispherical detectors for hard x-ray spectroscopy of kaonic atoms at the DAΦNE Collider *Sensors* **23** 7328
[12] Scordo A *et al* 2024 CdZnTe detectors tested at the DAΦNE collider for future kaonic atoms measurements *Nucl. Instrum. Methods A* **1060** 169060
[13] Artibani F *et al* 2024 new opportunities in kaonic atoms spectroscopy with novel czt detector *Frascati Phys. Ser.* **76** 96–102 (available at: https://inspirehep.net/files/ce13e3448c69f3a0f116b136050322f8#page=104)
[14] Artibani F *et al* 2025 Tests of new CZT detectors at DAΦNE collider for kaonic atoms measurements *Proc. Sci.* **DISCRETE2024** 031
[15] Milardi C *et al* 2009 Present status of the DAFNE upgrade and perspectives *Int. J. Mod. Phys. A* **24** 360–8
[16] Milardi C *et al* 2018 Preparation activity for the SIDDHARTA-2 run at DAΦNE *9th Int. Particle Accelerator Conf.* pp IPAC2018
[17] Milardi C *et al* 2021 DAΦNE commissioning for SIDDHARTA-2 experiment *J. Accel. Conf.* **IPAC2021** TUAB001
[18] Milardi C *et al* 2024 DAFNE operation strategy for the observation of the kaonic deuterium *J. Accel. Conf.* **IPAC2024** WER17
[19] Curceanu C *et al* 2020 Kaonic atoms to investigate global symmetry breaking *Symmetry* **12** 547
[20] Cieplý A, Mai M, Meißner U-G and Smejkal J 2016 On the pole content of coupled channels chiral approaches used for the $\bar{K}N$ system *Nucl. Phys. A* **954** 17–40
[21] Óbertovà J, Friedman E, Mareš J and Ramos A 2022 On K^--nuclear interaction, K^--nuclear quasibound states and K^- atoms *EPJ Web Conf.* **271** 07003
[22] Merafina M, Saturni F G, Curceanu C, Grande R D and Piscicchia K 2020 Self-gravitating strange dark matter halos around galaxies *Phys. Rev. D* **102** 083015
[23] Tolos L and Fabbietti L 2020 Strangeness in nuclei and neutron stars *Prog. Part. Nucl. Phys.* **112** 103770
[24] Hartmann F J 1990 *Exotic Atom Cascade Processes in Atoms With Z 2* (Springer) pp 127–39
[25] Gotta D 2004 Precision spectroscopy of light exotic atoms *Prog. Part. Nucl. Phys.* **52** 133–95
[26] Sgaramella F *et al* 2025 High precision x-ray spectroscopy of kaonic neon *Phys. Lett. B* **865** 139492
[27] Bassetti M, Biagini M, Biscari C, Guiducci S and Rosaria M M 1998 Daϕne main ring optics 01
[28] Boscolo M, Biagini M E, Guiducci S and Raimondi P 2007 Touschek background and beam lifetime studies for the DAFNE upgrade *Conf. Proc. C* **070625** 1454
[29] Miliucci M *et al* 2021 Silicon drift detectors system for high-precision light kaonic atoms spectroscopy *Meas Sci. Technol.* **32** 095501
[30] Miliucci M *et al* 2022 Large area silicon drift detectors system for high precision timed x-ray spectroscopy *Meas. Sci. Sci. Technol.* **33** 095502
[31] Khreptak A and Skurzok M 2023 Efficiency analysis and promising applications of silicon drift detectors *Bio. Algorithms Med. Syst.* **19** 74–79
[32] Sirghi F *et al* 2024 SIDDHARTA-2 apparatus for kaonic atoms research on the DAϕNE collider *J. Instrum.* **19** 11006
[33] Skurzok M *et al* 2020 Characterization of the SIDDHARTA-2 luminosity monitor *J. Instrum.* **15** 10010
[34] Abbene L *et al* 2024 First stability characterization for a CZT detection system in an e^+e^- collider environment *Sensors* **24** 7562
[35] Santos J P, Parente F, Boucard S, Indelicato P and Desclaux J P 2005 x-ray energies of circular transitions and electron screening in kaonic atoms *Phys. Rev. A* **71** 032501
[36] Gysel M, Lemberge P and Van Espen P 2003 Implementation of a spectrum fitting procedure using a robust peak model *x-ray Spectrom.* **32** 434–41
[37] Bazzi M *et al* 2011 A new measurement of kaonic hydrogen x-rays *Phys. Lett. B* **704** 113–7
[38] Sgaramella F *et al* 2024 Characterization of the SIDDHARTA-2 setup via the kaonic helium measurement *Condens. Matter* **9** 16
[39] Abbene L *et al* 2023 New opportunities for kaonic atoms measurements from CdZnTe detectors *Eur. Phys. J. ST* **232** 1487–92